https://doi.org/10.5607/en22007
Exp Neurobiol. 2022 Apr;31(2):116-130.
pISSN 1226-2560 • eISSN 2093-8144

Original Article

Experimental Neurobiology

Deletion of Phospholipase C β1 in the Thalamic Reticular Nucleus Induces Absence Seizures

Bomi Chang[1,2,3], Junweon Byun[1], Ko Keun Kim[1], Seung Eun Lee[2], Boyoung Lee[1], Key-Sun Kim[2], Hoon Ryu[2], Hee-Sup Shin[1]* and Eunji Cheong[3]*

[1]Center for Cognition and Sociality, Institute for Basic Science, Daejeon 34126,
[2]Brain Science Institute, Korea Institute of Science and Technology, Seoul 02792,
[3]Department of Biotechnology, College of Life Science and Biotechnology, Yonsei University, Seoul 03722, Korea

Absence seizures are caused by abnormal synchronized oscillations in the thalamocortical (TC) circuit, which result in widespread spike-and-wave discharges (SWDs) on electroencephalography (EEG) as well as impairment of consciousness. Thalamic reticular nucleus (TRN) and TC neurons are known to interact dynamically to generate TC circuitry oscillations during SWDs. Clinical studies have suggested the association of *Plcβ1* with early-onset epilepsy, including absence seizures. However, the brain regions and circuit mechanisms related to the generation of absence seizures with *Plcβ1* deficiency are unknown. In this study, we found that loss of *Plcβ1* in mice caused spontaneous complex-type seizures, including convulsive and absence seizures. Importantly, TRN-specific deletion of *Plcβ1* led to the development of only spontaneous SWDs, and no other types of seizures were observed. *Ex vivo* slice patch recording demonstrated that the number of spikes, an intrinsic TRN neuronal property, was significantly reduced in both tonic and burst firing modes in the absence of *Plcβ1*. We conclude that the loss of *Plcβ1* in the TRN leads to decreased excitability and impairs normal inhibitory neuronal function, thereby disrupting feedforward inhibition of the TC circuitry, which is sufficient to cause hypersynchrony of the TC system and eventually leads to spontaneous absence seizures. Our study not only provides a novel mechanism for the induction of SWDs in *Plcβ1*-deficient patients but also offers guidance for the development of diagnostic and therapeutic tools for absence epilepsy.

Key words: Thalamocortical neuronal system, Absence seizure, Spike and wave discharges, Thalamic reticular nucleus, *Plcβ1*

INTRODUCTION

Absence seizures refer to nonconvulsive status epilepticus (NCSE) caused by abnormal synchronized oscillations in the thalamocortical (TC) circuit, which result in widespread spike-and-wave discharges (SWDs) on electroencephalography (EEG) along with impairment of consciousness [1]. Symptomatically, there are two essential diagnostic components of absence seizures, behavioral arrest during the clinical ictal state, with severe impairment of consciousness, and signs of SWDs on EEG that spread throughout the brain [2]. The frequency of hypersynchrony ranges from 2.5 to 4 Hz, gradually decreasing over time, and the seizures usually last for up to 15~20 s [3]. The age of onset ranges from 4 and 7 years [4], and cognitive impairment can develop if a diagnosis is not made in a timely manner [5, 6]. In most cases, absence seizures disappear during adolescence. However, they sometimes progress to longer or more intense seizures, which can be prevented by earlier diagnosis and treatment [7, 8]. Therefore, understanding the cellular mechanisms and identifying genetic risk factors underlying the pathogenesis of absence epilepsies are necessary for the development of appropriate diagnostic and therapeutic tools [9].

The thalamic reticular nucleus (TRN) plays a significant role in controlling TC circuits and SWD generations. The TRN is a shell-

Submitted February 24, 2022, Revised March 22, 2022,
Accepted April 5, 2022

*To whom correspondence should be addressed.
Eunji Cheong, TEL: 82-2-2123-5885, FAX: 82-2-362-7265
e-mail: eunjicheong@yonsei.ac.kr
Hee-Sup Shin, TEL: 82-42-878-9155, FAX: 82-42-878-9151
e-mail: shin@ibs.re.kr

like structure comprising GABAergic neurons that cover most of the rostral, lateral, and ventral parts of the thalamus [10] and provide major inhibitory synaptic input to the TC neurons [11, 12]. TRN neurons generate two distinctive patterns of action potential firings, tonic and burst. Tonic modulation of the TRN has been implicated in the genesis of absence seizures [13, 14]. Moreover, rhythmic burst firing mediated by T-type channels in TRN neurons is critical for the generation of TC oscillations during SWDs [2, 15, 16]. More importantly, a recent study suggested that altered intrinsic excitability of TRN neurons and disruption of TRN–TRN synaptic inhibition are sufficient to regulate thalamic and cortical network synchrony and generate absence seizures [14]. Therefore, TRN neurons can serve as a central modulator of TC network states and of absence seizure generation.

The *Plcβ1* enzyme that catalyzes the formation of inositol 1,4,5-trisphosphate (IP3) and diacylglycerol (DAG) from phosphatidylinositol 4,5-bisphosphate (PIP2). This reaction requires calcium as a cofactor and activates multiple signaling pathways and gene expression changes [17, 18]. *Plcβ1* is expressed throughout cortical layers II~VI of the brain and is preferentially expressed in the TRN of the thalamus [19-21]. It plays an important role in modulating diverse developmental and functional aspects of the central nervous system. Likewise, *Plcβ1* deficiency is associated with human epilepsy during infancy and childhood. Although different cases show distinct characteristic phenotypes, most patients with *Plcβ1* deficiency show the five common features of early-onset epileptic encephalopathy (EOEE): (1) seizure onset in infancy and seizures heralded by an arrest of activity followed by staring; (2) pharmacoresistant seizures; (3) abnormalities on EEG; (4) neurological/developmental regression associated with seizures; and (5) long-term cognitive and motor neurodevelopmental impairment [22-24]. Preclinical studies have consistently shown that *Plcβ1* homozygous knockout (KO) mice exhibit early-onset severe tonic seizures and growth retardation [25]. These clinical and preclinical studies have suggested an important function of *Plcβ1* in early-onset epilepsy, including absence seizures.

In this study, we found that *Plcβ1* deficiency generated spontaneous complex types of seizures, including convulsive and absence seizures. Interestingly, the TRN-specific deletion of *Plcβ1* generated only spontaneous SWDs, leading to the development of absence seizures. Slice patch recording demonstrated that both the tonic and burst firing of TRN neurons were significantly reduced in $Plcβ1^{-/-}$ mice. Altogether, the results of our study not only suggest a novel role of *Plcβ1* in the TRN underlying the generation of SWDs but also offer guidance for the development of diagnostic and therapeutic tools for absence epilepsy.

MATERIALS AND METHODS

Animals

The mice were housed at room temperature (22℃), fed *ad libitum* and maintained under a 12 h light/dark cycle. For slice recording, mice were used at the age of 20-28 days, while ~16-week-old male mice were used for EEG recording. A C57BL/6J inbred glutamate decarboxylase 65 (GAD2)-green fluorescence protein (GFP) knock-in line was imported from Jackson Laboratory (JAX Mice and Services, Bar Harbor, ME, USA). Adult male $Plcβ1^{-/-}$ and wild-type littermate mice on a B6×129 F1 background were obtained by mating parental-strain C57BL/6J (N18-20) $Plcβ1^{+/-}$ mice and 129S4/SvJae (N18-20) $Plcβ1^{+/-}$ mice. The $Plcβ1^{+/-}$/$GAD65GFP^{tg}$ mice were maintained on the129S4/SvJae and C57BL/6 genetic backgrounds and mated to derive the following F1 progeny: B6129 $Plcβ1^{+/-}$/$GAD65GFP^{tg}$, B6129 $Plcβ1^{+/-}$/$GAD65GFP^{tg}$, and B6129 $Plcβ1^{-/-}$/$GAD65GFP^{tg}$. The GFP genotypes were determined by direct visualization of fluorescence at the age of 1~4 days. Genotypes were determined by PCR analysis using the primers listed in Supplementary Table 1. *Plcβ1* conditional knockout (cKO, $Plcβ1^{f/f}$, N18-20) was validated by PCR analysis. *SST-ires-Cre* mice were obtained from the Korean Institute for Science and Technology [26, 27]. Animal care and handling were performed in accordance with the guidelines of the Institutional Animal Care and Use Committee of the Institute for Basic Science (IBS).

EEG electrode implantation and recording

Skull surface screw electrodes for EEG recording were implanted at the following coordinates in mice under 16 weeks of age that were anesthetized with ketamine using a stereotaxic device (David Kopf Instruments): anteroposterior (AP), -1.5 mm; mediolateral (ML), +1.5 mm; AP, -1.3 mm; and ML, +1.3 mm. The ground electrode was implanted in the skull above the occipital region of the brain. For EMG signal recording, a Teflon-coated tungsten electrode was inserted into the neck muscle to record postural tone. The animals were allowed to fully recover for 7 days before the experiments. We recorded EEG and EMG signals in all the groups using a monopolar setting in real time (sampling frequency, 500 Hz). EEG activity was recorded for 60 min using a pClamp10. All EEGs were acquired using an analog amplifier (8~16℃, Grass Technologies) and digitized by an analog-digital converter (Axon Digidata 1320A, Molecular Devices). Each signal was band-pass filtered using a digital Butterworth filter with a cutoff frequency of 0.5 and 30 Hz.

EEG data analysis and SWD criteria

We classified SWDs based on two criteria: (1) the amplitude of SWDs was required to be greater than twice the amplitude of EEG waveforms observed during the awake state, and (2) the duration of SWDs was required to be at least 0.5 s. pClamp10 and MATLAB were utilized to detect SWDs based on the amplitudes, peak-to-peak periods, and shapes of EEG signals. We applied a resolution of 250 ms and a frequency range of 2~7 Hz for detection. Waveforms with a low total power and non-SWD harmonic and high-frequency content were filtered automatically. Temporal spectrograms were obtained by filtering the signals with a second-order Butterworth infinite impulse response (IIR) via a high-pass filter with a cutoff frequency before fast Fourier transformation. The power spectrum was normalized frequency-wise from the mean baseline power density estimated between the first and tenth minute of the baseline recording. In this study, we mainly focused on the role of PLCβ1 in absence seizures, so we attempted to exclude EEG recordings during convulsive seizures to analyze and carefully examine SWDs.

AAV-shRNA construct design and virus strains

To design the AAV-sh*Plcβ1* vector for the knockdown (KD) experiment, we used the previously verified target sequence 5'-CCTCCAGTGAGGAGA-TAGAAA-3'. The scrambled shRNA (shSCR) sequence 5'AATCGCATAGCGTATGCCGTT-3' was used to construct a nontargeting control virus [28]. AAV-mCherry was determined to have a titer of 3.92×10^{10} genome copies per milliliter (GC/ml). To conditionally knock out the *Plcβ1* gene in floxed *Plcβ1* mice, the AAV9.hSyn.HI.GFP-Cre.WPRE. SV40 virus (University of Pennsylvania) was used. The control virus (AAV9. hSyn.eGFP.WPRE.bGH) was also injected into floxed *Plcβ1* mice.

Viral vector and CTB injection

In in vivo tests for selective *Plcβ1* KD and cKO, AAV vectors concentrated to high titers (3.92×10^{10} GC/ml) were prepared and microinjected bilaterally into the ventromedial (vm) TRN region (anteroposterior/mediolateral/dorsoventral (AP/ML/DV) -1.10/±1.80/-3.00 mm) with a pressure injection tool (Parker Hannifin Corp., Picospritzer III). The retrograde tracer CTB (0.5% diluted in distilled water; List Biological) was injected by iontophoresis (7/7 s on/off duty cycle, 1 μA) into the VB regions (AP/ML/DV, -1.45/+1.60/-3.60 mm).

Immunohistochemistry

Immunohistochemistry analysis was performed as described previously [13] using the following primary antibodies: anti-PLCβ1 (mouse, 1:300; Santa Cruz), anti-PV (mouse, 1:3,000~5,000; Swant, 235) and anti-cholera toxin-B subunit (goat, 1:20,000~30,000). The secondary antibodies included Alexa 488, Cy3, and Cy5 (1:500, Jackson ImmunoResearch), and images were captured using a confocal laser scanning system (Nikon).

Brain slice preparation

Slice preparation was performed as described previously [13]. For patch-clamp recordings, 20- to 28-day-old mouse brains were quickly removed and placed in carbogen-equilibrated ice-cold slicing solution containing 2.5 mM KCl, 10 mM $MgSO_4$, 1.25 mM NaH_2PO_4, 24 mM $NaHCO_3$, 0.5 mM $CaCl_2$-$2H_2O$, 11 mM glucose, and 234 mM sucrose. From dorsal to ventral, 270-μm-thick brain slices containing the TRN region were selectively collected and incubated in an ACSF solution containing 125 mM NaCl, 2.5 mM KCl, 5 mM $MgSO_4$, 1.25 mM NaH_2PO_4, 26 mM $NaHCO_3$, 3 mM $CaCl_2$-$2H_2O$, and 25 mM glucose for 30 min before recording.

Electrophysiology

In K^+-based whole-cell current clamp mode, the intrinsic firing properties were measured in recording solutions comprising 125 mM NaCl, 2.5 mM KCl, 1.3 mM $MgCl_2$, 1.25 mM NaH_2PO_4, 26 mM $NaHCO_3$, 2 mM $CaCl_2$-$2H_2O$, and 25 mM glucose [310~320 mOsm/L] bubbled with 95% (vol/vol) O_2/5% (vol/vol) CO_2 at 36℃. The solution heater was used to maintain the temperature at 36℃ during recording solution perfusion. Recording electrodes were pulled from fabricated standard-wall borosilicate glass capillary tubes (G150F-4: outer diameter (OD), 1.50 mm; inner diameter (ID), 0.86 mm; Warner Instruments) and had a 4~7 MΩ tip resistance when filled with an intracellular solution containing 140 mM K-gluconate, 0.1 mM $CaCl_2$, 1 mM $MgCl_2$, 10 mM HEPES, 0.02 mM EGTA, and 4 mM Mg-ATP [(pH 7.2) 300~310 mOsm/L]. Recordings of Ca^{2+} currents in intact TRN neurons in slices were performed as described previously. Brain slices were superfused with a bathing solution containing 120 mM NaCl, 20 mM tetraethylammonium (TEA)-Cl, 5 mM CsCl, 3 mM KCl, 2 mM $MgCl_2$, 10 mM HEPES, 2.5 mM $CaCl_2$-$2H_2O$, 1 mM 4-amino pyridine (4-AP), and 0.001 mM tetrodotoxin (TTX) bubbled with 95% O_2/5% CO_2 at 36℃. The electrode solution contained 117 mM Cs-gluconate, 13 mM KCl, 10 mM TEA-Cl, 1 mM $MgCl_2$, 0.07 mM $CaCl_2$-$2H_2O$, 10 mM HEPES, 10 mM 1,2-bis(o-amino phenoxy)ethane-N,N',N'-tetraacetic acid, 4 mM Mg-ATP, and 0.3 Na-GTP; the pH was adjusted to 7.35 with CsOH, and the osmolarity was adjusted to 290 mosmol/L.

The series resistance compensation function (>60%) was used routinely, with a final access resistance of ~30 MΩ. The currents were corrected for capacitive currents and leak currents using

https://doi.org/10.5607/en22007

a P/4 leak subtraction protocol. Twenty to thirty minutes were required to achieve acceptable perforation, with final series resistances ranging from 15 to 30 MΩ. The membrane holding potential was -60 mV unless otherwise specified.

Statistical analysis

Data acquisition and analysis were performed using pClamp10, MATLAB (MathWorks) and GraphPad Prism (GraphPad Software, San Diego, USA) in combination. We performed one-way repeated ANOVA and Bonferroni post hoc analysis of the electrophysiological experimental results using comparisons between groups and within-subject repeated conditions, including the temporal evolution of SWD density (i.e., main factors of group and time and Group×Time interaction). Large (>10 mice) and small sample size comparisons were performed using the two-tailed Student's t test and Wilcoxon rank-sum test, respectively. All data are presented as the mean±SEM unless stated otherwise.

RESULTS

Plcβ1-deficient mice exhibit complex abnormal EEG patterns

To understand the role of *Plcβ1* in absence seizures, we utilized F1 (C57BL/6J×129S4/SvJae) *Plcβ1*$^{-/-}$ (F1 *Plcβ1*$^{-/-}$) mice that show normal survival. We measured EEG and EMG signals from F1 *Plcβ1*$^{-/-}$ mice to detect neural activity and found that F1 *Plcβ1*$^{-/-}$ mice exhibited a mixture of abnormally synchronized oscillations on EEG with spontaneous absence seizures. In additional behavioral analyses (data not shown), F1 *Plcβ1*$^{-/-}$ mice show absence seizures as well as convulsive seizures. Thus, we tried to avoid the EEG recordings during convulsive seizures. The EEG power spectrogram exhibited high power spectrum density (PSD) in the 0~10 Hz frequency range (Fig. 1A). The peak spectral power of F1 *Plcβ1*$^{-/-}$ SWD events occurred at 3.5 Hz (Fig. 1B). Absence seizures detectable on the EEG pattern of SWDs occurred 130±8 times per hour, with an average duration of 1.5±0.2 s per minute. Behavior was monitored by EMG signals, and low EMG signals in *Plcβ1* KO mice were observed during SWDs, indicating the absence of seizure generation (Fig. 1C, D). Next, we assessed the effect of ethosuximide (ETX), a known anti-absence epilepsy drug [29, 30], on our model. The SWDs in F1 *Plcβ1*$^{-/-}$ mice decreased substantially after the i.p. injection of ETX (200 mg/kg, 78.5±9 times), whereas injection of saline had no effect (140±7 times) (Fig. 1E). Altogether, F1 *Plcβ1*$^{-/-}$ mice exhibit complex abnormal EEG patterns. Next, we explored the specific brain regions involved in the generation of SWDs caused by *Plcβ1* deficiency.

Selective Plcβ1 deletion in the ventromedial TRN induces absence seizures

To separate the role of *Plcβ1* in absence seizures from convulsive seizures, we focused on the TRN, a central modulator of TC network states and of absence seizure generation. Importantly, *Plcβ1* is highly expressed in this brain region. First, to confirm the anatomical projection pattern of TRN neurons to TC relay nuclei, we injected cholera toxin subunit B (CTB) 488, a retrograde dye, into the ventrobasal (VB) region (Fig. 2A), including the ventroposteromedial (VPM) and ventroposterolateral (VPL) regions, to identify input signals from the TRN [10]. Because the majority of TRN neurons are parvalbumin (PV)- and somatostatin (SST)-positive, we used PV immunostaining [31, 32] and *Sst-Cre;Ai14* mice for precise validation within the TRN to examine the cell type–specific projections of TRN neurons to the VB thalamus. We detected CTB-488 signals mainly in the vmTRN three days after injection (Fig. 2B), indicating that vmTRN neurons send inhibitory projections to TC neurons in the VB [10]. Moreover, approximately 50% of the CTB-488-positive cells in the vmTRN expressed both PV and SST, indicating that no distinct cell types projected from the vmTRN to TC neurons in the VB region (Fig. 2C).

To specifically delete *Plcβ1* in the vmTRN, we injected an AAV vector expressing Cre recombinase into the vmTRN of B6 *Plcβ1* conditional knockout (cKO) mice (*Plcβ1* cKO). The mice injected with GFP control expression vectors were used as a control group (Fig. 2D). Immunohistochemistry staining confirmed the deletion of *Plcβ1* in the vmTRNs of *Plcβ1* cKO mice (Fig. 2D). Three weeks after the injection, the mice in both groups underwent EEG recording for 14 successive days. Unlike the *Plcβ1*$^{-/-}$ group, which exhibited PSD in the 0~12 Hz frequency range, the *Plcβ1* cKO group exhibited low PSD at 5~12 Hz (Fig. 2E, F). The remaining EEG power in the 0~5 Hz frequency range indicated only SWDs in the *Plcβ1* cKO group (Fig. 2G). The number and duration of SWDs in the *Plcβ1* cKO group were significantly higher than those in the control group but were still similar to those in the *Plcβ1*$^{-/-}$ group. In the *Plcβ1* cKO group, 153±8 SWDs occurred every hour, and the average duration was 1.7±0.2 s per minute. There was no significant difference in the number of SWDs among *Plcβ1*$^{+/+}$, *Plcβ1*$^{+/-}$, and GFP control mice (GFP). Notably, the numbers of SWDs between *Plcβ1*$^{-/-}$ and cKO mice were similar, indicating that the specific deletion of *Plcβ1* in the vmTRN was sufficient to induce SWDs (Fig. 2H). *Plcβ1* cKO mice did not show convulsive seizures (data not shown).

With another strategy to confirm the selective role of *Plcβ1* in the vmTRN in absence seizure generation, shRNA targeting *Plcβ1* or scrambled control (pAAV2-sh *Plcβ1*-mCherry or pAAV2-scram-mCherry) were injected into the vmTRN of F1 mice to

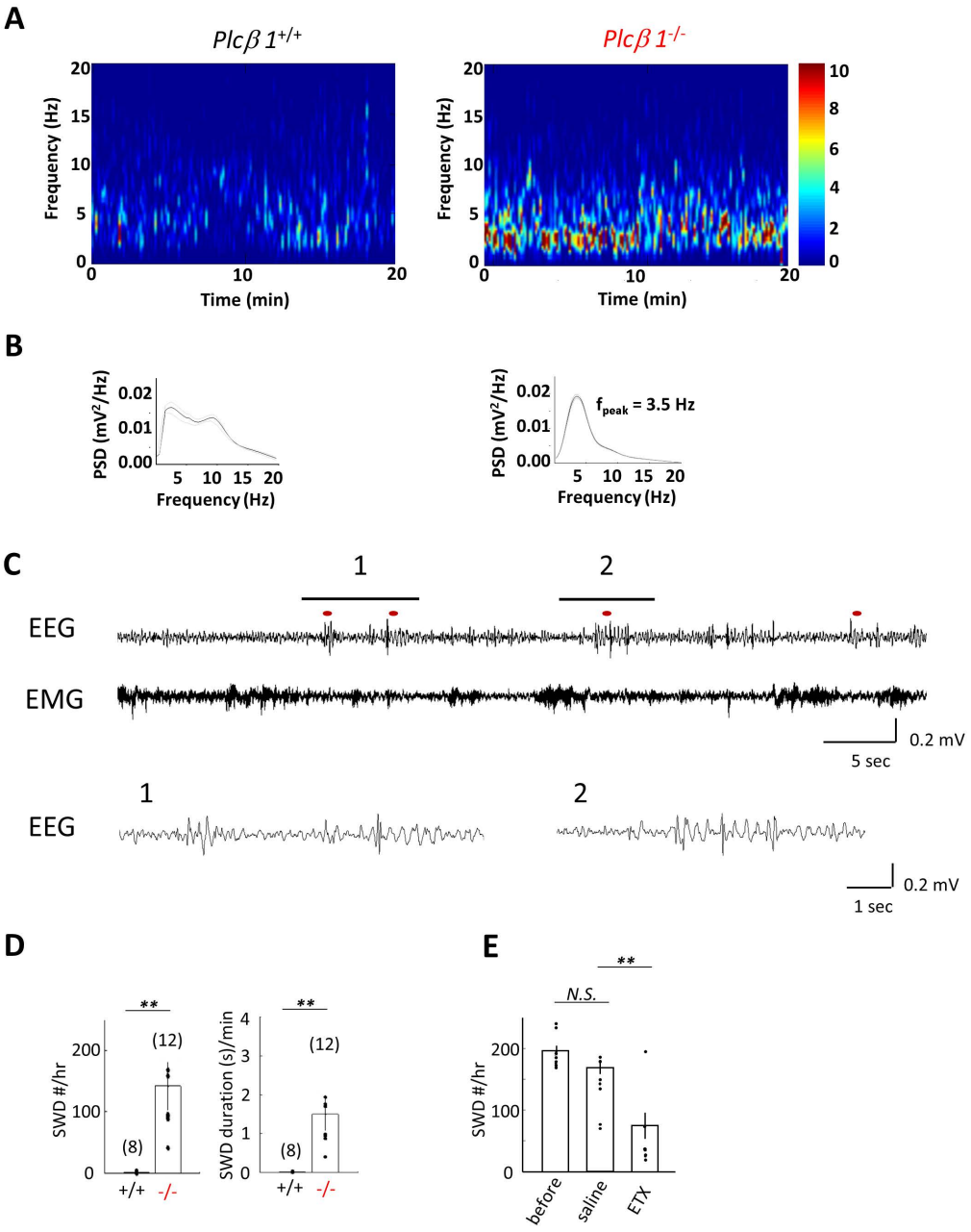

Fig. 1. *Plcβ1*-deficient mice exhibit complex abnormal EEG patterns. (A) Average EEG power spectrograms of *Plcβ1*$^{+/+}$ and *Plcβ1*$^{-/-}$ mice during a 20 min recording. (B) Power analysis of spontaneous SWDs in *Plcβ1*$^{-/-}$ mice showed a peak frequency at 3.5 Hz. (C) Representative EEG and EMG traces from *Plcβ1*$^{+/+}$ and *Plcβ1*$^{-/-}$ mice. Synchronized SWDs were observed in the frontal cortices of *Plcβ1*$^{-/-}$ mice. (D) Summary graphs of the total numbers (left) and average durations (right) of SWDs in *Plcβ1*$^{+/+}$ and *Plcβ1*$^{-/-}$ mice; two-tailed Student's t test. (E) Comparison of the number of SWDs before and after ETX administration. Data are presented as the mean±SEM ($^{n.s}$p>0.05, *p<0.001, **p<0.05; two-tailed Student's paired t test). For all data, n=8 for the control group and n=12 for the *Plcβ1*$^{-/-}$ group.

knock down *Plcβ1* expression locally (Fig. 3A). Similarly, the *Plcβ1* KD group exhibited low PSD at 5~12 Hz (Fig. 3B). The remaining EEG power in the 0~5 Hz frequency range indicated only SWDs in the *Plcβ1* KD group (Fig. 3B, C). The KD mice exhibited a peak frequency at 3.25 Hz (Fig. 3D). The number of SWDs in KD mice was similar to those in *Plcβ1*$^{-/-}$ and cKO mice, confirming that the specific deletion of *Plcβ1* in the vmTRNs of mice on either the B6 or F1 background was sufficient to induce SWDs (Fig. 3E). *Plcβ1* KD mice did not show convulsive seizures (data not shown).

https://doi.org/10.5607/en22007

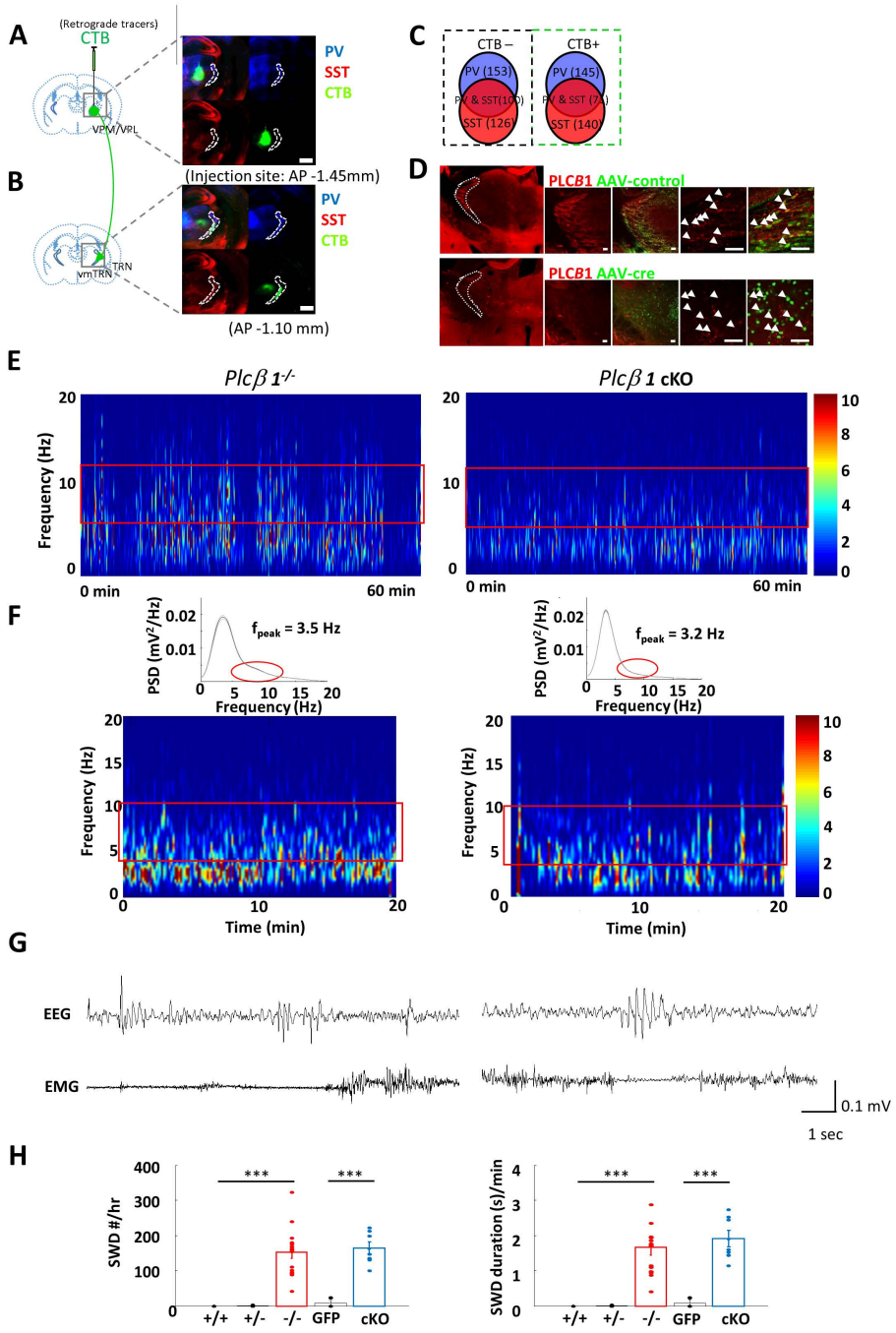

Fig. 2. Selective *Plcβ1* deletion in the ventromedial (vm) TRN induces absence seizures. (A) Left, schematic depiction of CTB injection. Right, PV and SST immunostaining at the CTB injection site. The white boundary represents the anterior TRN. Scale bar, 50 μm. (B) Left, retrograde labeling of neurons projecting from the vmTRN to TC neurons. Right, PV and SST immunostaining of CTB signals in the vmTRN (inside white boundary). Scale bar, 50 μm. (C) Population of PV- and SST-expressing cells in vmTRN neurons. The left square represents CTB-negative neurons, and the right square represents CTB-positive neurons (D) The expression of PLCβ1 was not affected by the injection of AAV-control (GFP) into the vmTRN regions (upper). The expression of PLCβ1 was greatly reduced by the injection of AAV-syn-cre into the vmTRN regions of B6 *Plcβ1* conditional knockout mice (cKO) (lower). Scale bar: 50 μm. (E) Average EEG power spectrogram of cKO mice. The red square indicates the 5~15 Hz frequency range. (F) Power analysis in spectrogram. *Plcβ1*$^{-/-}$ mice showed a peak frequency at 3.5 Hz, and Plcβ cKO mice showed a peak frequency at 3.2 Hz. The red block indicate the disappearance of the frequency range (5~12 Hz). (G) Representative EEG and EMG traces from *Plcβ1*$^{-/-}$ and cKO mice. (H) Summary graphs of the total numbers (left) and average durations (right) of SWDs in *Plcβ1*$^{+/+}$ (n=8), $^{+/-}$ (n=10), $^{-/-}$(n=12), GFP (n=9), and cKO (n=10) mice. The values in the *Plcβ1*$^{+/+}$, *Plcβ1*$^{+/-}$ and GFP groups did not significantly differ from each other. The values in the *Plcβ1*$^{-/-}$ and cKO groups did not significantly differ from each other, while those in the *Plcβ1*$^{-/-}$ and cKO groups were significantly different from those in the *Plcβ1*$^{+/+}$, *Plcβ1*$^{+/-}$ and GFP groups. The data are presented as the mean±SEM, one-way ANOVA, ***p<0.001, post hoc (Bonferroni).

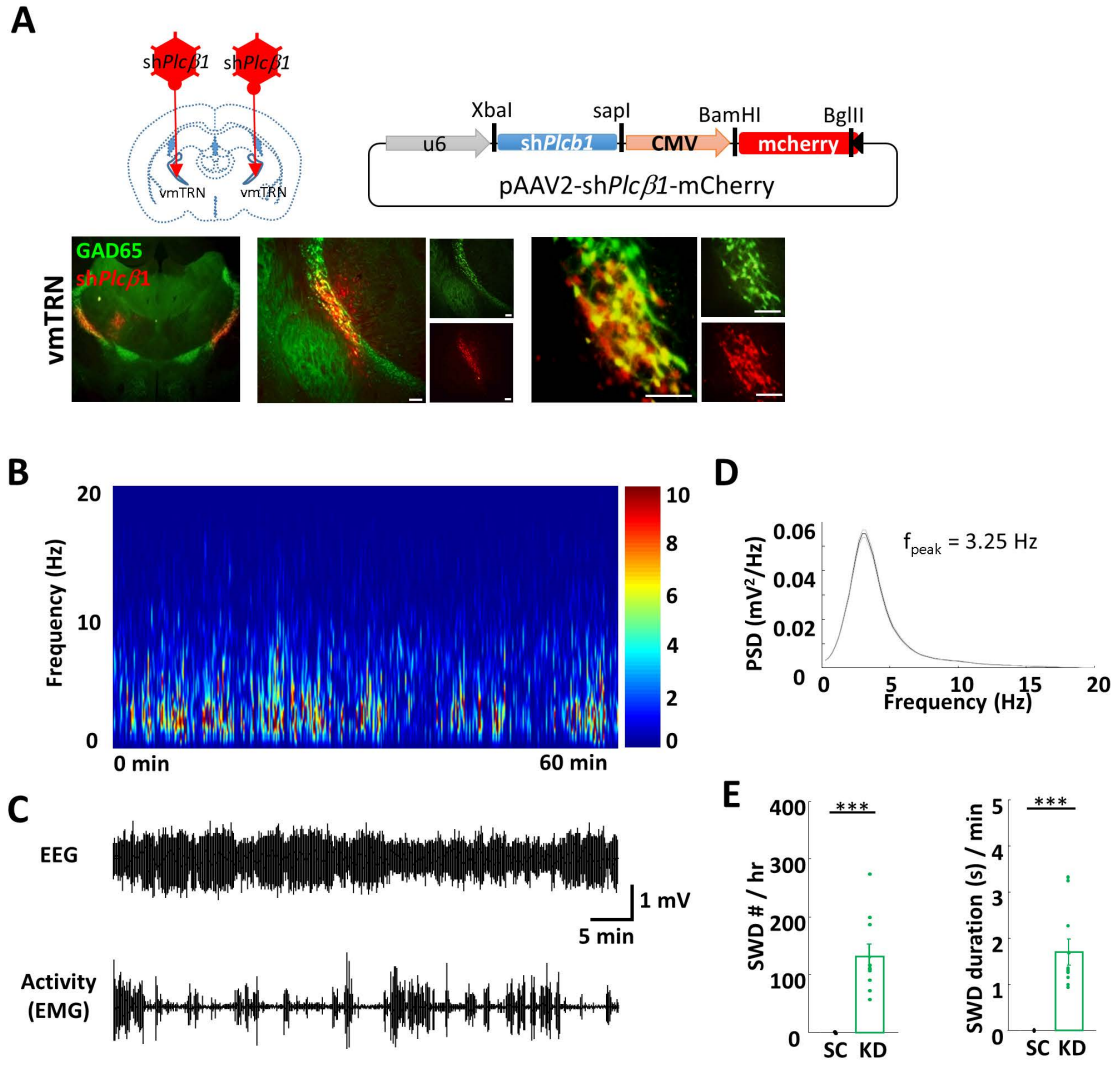

Fig. 3. Selective knockdown (KD) of *Plcβ1* in the vmTRN induces absence seizures. (A) Scheme of selective KD of *Plcβ1* in the vmTRN. Left, vmTRN injection site (AP -1.1, ML ±1.8, DV -3.0). Right, schematic representation of the targeting vector for KD virus. Bottom, microinjection of the AAV-sh*Plcβ1*-mCherry virus into the vmTRNs of GAD65GFP transgenic mice. Scale bar, 50 μm. (B) Average EEG power spectrograms of *Plcβ1*$^{+/-}$ and *Plcβ1* KD mice. (C) Representative EEG and EMG traces from *Plcβ1* KD mice. (D) Power analysis of spontaneous SWDs. *Plcβ1* KD mice showed a peak frequency at 3.25 Hz. (E) Summary graphs of the total numbers (left) and average durations (right) of SWDs in scrambled (n=9), and *Plcβ1* KD (n=13) mice. The values in the KD group was significantly different from in the SC group. The data are presented as the mean±SEM, one-way ANOVA, ***p<0.001, post hoc (Bonferroni).

Both tonic and burst firings of the vmTRN are decreased in Plcβ1$^{-/-}$ *mice*

To determine whether the intrinsic properties of TRN neurons were altered upon deletion of the *Plcβ1* gene, generation of action potentials (APs) in response to current injection were measured using patch-clamp recordings. TRN neurons control the state of consciousness by generating distinctive patterns of AP firing, namely, tonic and burst firing. We generated *Gad65-GFP*^{tg}; *Plcβ1*$^{-/-}$ mice to visualize the *Gad65*-positive neurons in the vmTRN for patch-clamp recordings (Fig. 4A). For the tonic firing pattern, depolarizing current steps (10 pA increments, ten steps, 1 s duration) were injected from a holding potential of -60 mV close to the resting membrane potential (Fig. 4B). We found that the frequency of tonic firings was significantly reduced in *Plcβ1*$^{-/-}$ mice compared to wild-type mice (Fig. 4C). The spike height, spike half-width, and action potential threshold measured from the response to current steps were changed, consistent with a decrease in neuron excitability (Fig. 4D~F). Other passive electrical membrane properties of TRN neurons, including input resistance (R_i), membrane resistance (R_m), and resting membrane potential (Vm), did not differ between the mutant and wild-type groups

https://doi.org/10.5607/en22007

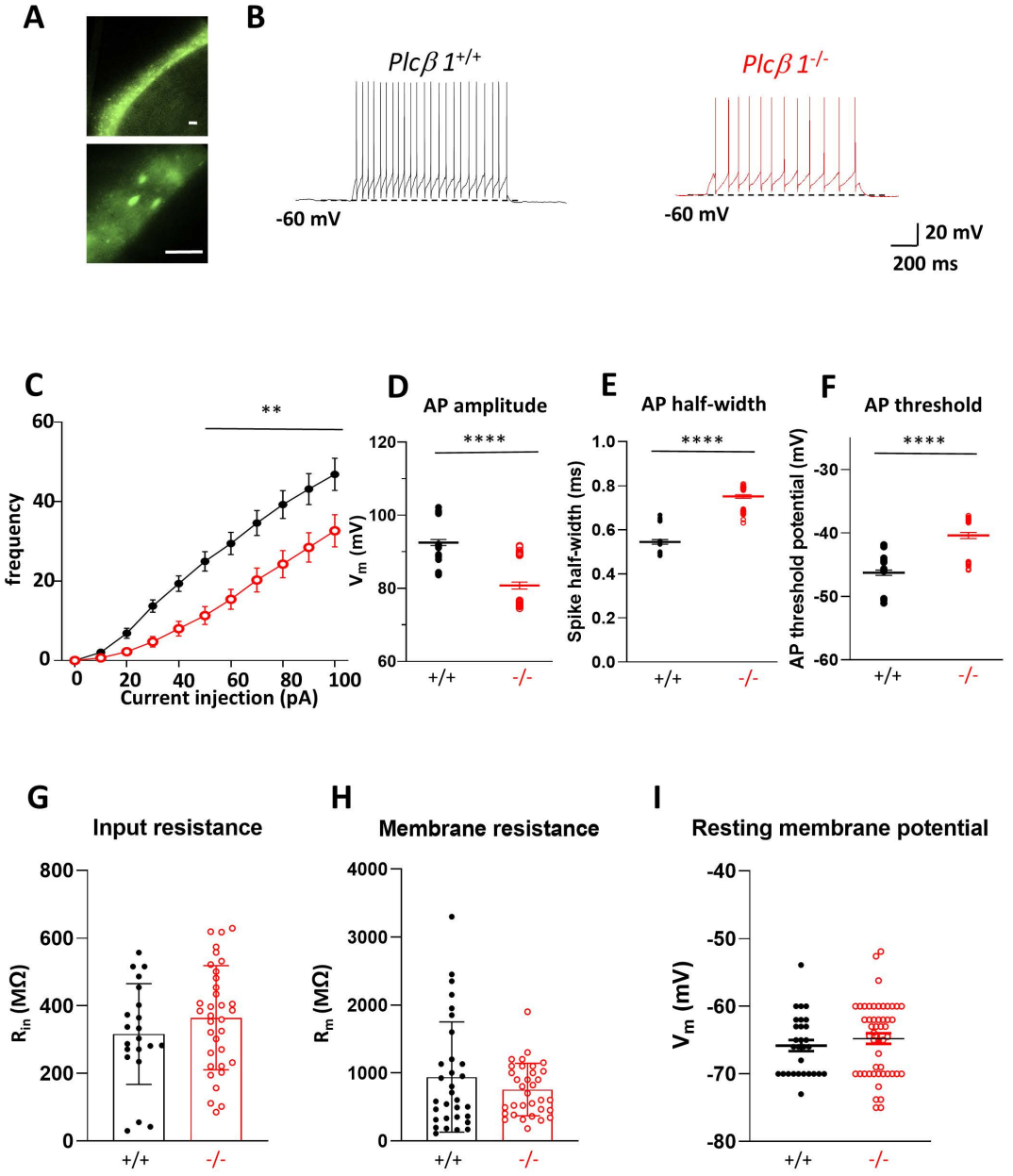

Fig. 4. Tonic firing of the vmTRN is decreased in *Plcβ1*$^{-/-}$ mice. (A) Recording of vmTRN neurons from *Gad65*-GFP^{tg}; *Plcβ1*$^{+/+}$ or *Gad65*-GFP^{tg}; *Plcβ1*$^{-/-}$ mice. (B) Representative traces of tonic firings in *Plcβ1*$^{+/+}$ (left) and *Plcβ1*$^{-/-}$ (right) vmTRN neurons. (C) Average number of tonic firings with different current pulses in *Plcβ1*$^{+/+}$ and *Plcβ1*$^{-/-}$ vmTRN neurons. (D) AP peak height: 92.5±2.0 and 80.8±2.0 mV in *Plcβ1*$^{+/+}$ and *Plcβ1*$^{-/-}$ mice, two-tailed, ****p<0.0001. (E) AP 1/2 width: 0.55±0.2 and 0.75±0.2 ms in *Plcβ1*$^{+/+}$ and *Plcβ1*$^{-/-}$ mice, two-tailed, ****p<0.0001. (F) AP threshold: -46.3±0.6 and -40.4±0.6 mV in *Plcβ1*$^{+/+}$ and *Plcβ1*$^{-/-}$ mice, two-tailed, ****p<0.0001. (G) Input resistance: 316.63±42 and 364.7±42 MΩ in *Plcβ1*$^{+/+}$ and *Plcβ1*$^{-/-}$, two-tailed, $^{n.s.}$ p=0.25. (H) Membrane resistance: 860.4±136 and 718±136 MΩ in *Plcβ1*$^{+/+}$ and *Plcβ1*$^{-/-}$ mice, two-tailed, $^{n.s.}$ p=0.30. (I) Resting membrane potential: -65.8±1.1 and 64.8±1.1 mV in *Plcβ1*$^{+/+}$ and *Plcβ1*$^{-/-}$ mice, two-tailed, $^{n.s.}$ p=0.38. All data are presented as the mean±SEM.

(Fig. 4G~I). Of the recorded TRN neurons, only data from inhibitory neurons with a membrane capacitance of less than 60 pF were analyzed [33].

For the burst firing pattern, in acute brain slices, the current injection hyperpolarized the membrane potential to -100 mV and followed by subsequent burst firing patterns (Fig. 5A). In *Plcβ1*$^{-/-}$ mice, both the total number of burst events and the number of burst spikes were significantly decreased compared to those in the wild-type mice (Fig. 5B, C). The spike height and action potential threshold did not differ between the mutant and wild-type groups (Fig. 5D, E). Taken together, these results demonstrated that both tonic and burst firings were significantly decreased in *Plcβ1*$^{-/-}$ mice, indicating

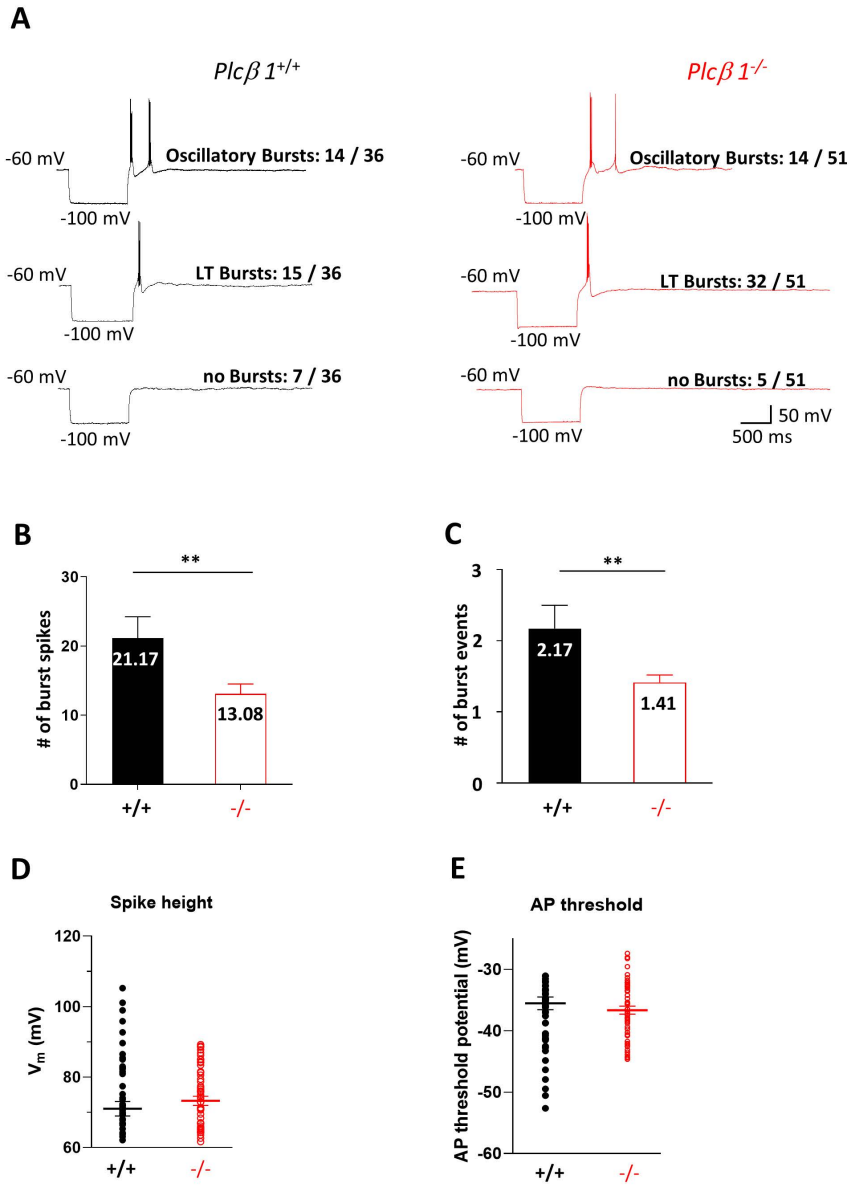

Fig. 5. Burst firing of the vmTRN is decreased in *Plcβ1*$^{-/-}$ mice. (A) Firing characteristics of *Plcβ1*$^{+/+}$ (left three traces) and *Plcβ1*$^{-/-}$ (right three traces) vmTRN neurons. (B) Number of burst spikes: 21.2±3 and 13.1±3 times in *Plcβ1*$^{+/+}$ and *Plcβ1*$^{-/-}$, two-tailed, **p<0.009. (C) Number of burst events: 2.2±0.3 and 1.4±0.3 times in *Plcβ1*$^{+/+}$ and *Plcβ1*$^{-/-}$ mice, two-tailed, *p<0.01. (D) AP spike height: 71.0±2.5 and 73.3±2.5 mV in *Plcβ1*$^{+/+}$ and *Plcβ1*$^{-/-}$ mice, two-tailed, n.s. p=0.36. (E) AP threshold potential: -35.5±1.2 and -36.6±1.2 mV in *Plcβ1*$^{+/+}$ and *Plcβ1*$^{-/-}$ mice, two-tailed, n.s. p=0.37. All data are presented as the mean±SEM.

that the deletion of *Plcβ1* reduced the excitability of TRN neurons.

Neither LVA nor HVA Ca^{2+} currents are altered in the vmTRNs of Plcβ1$^{-/-}$ *mice*

To understand the cellular mechanism underlying the decrease in TRN excitability in *Plcβ1*$^{-/-}$ mice, we investigated the possible role of calcium channels. T-type calcium channels in TRN and TC neurons are implicated in the generation of absence seizures [13]. We prepared acute brain slices for whole-cell voltage-clamp recording in the TRN neurons of *Plcβ1*$^{-/-}$ and wild-type mice between 21 and 28 days of age. High-voltage–activated (HVA) inward Ca^{2+} currents were evoked by depolarizing voltage steps from a holding potential of -60 mV to test potentials ranging from -50 mV to +40 mV (Fig. 6A) [34, 35]. Under these conditions, most low-voltage–activated (LVA) Ca^{2+} channels should have remained inactivated. The peak current density at each test potential did not differ in the TRN neurons of *Plcβ1*$^{-/-}$ mice compared to those of wild-type mice. There was no significant difference in the normal-

https://doi.org/10.5607/en22007

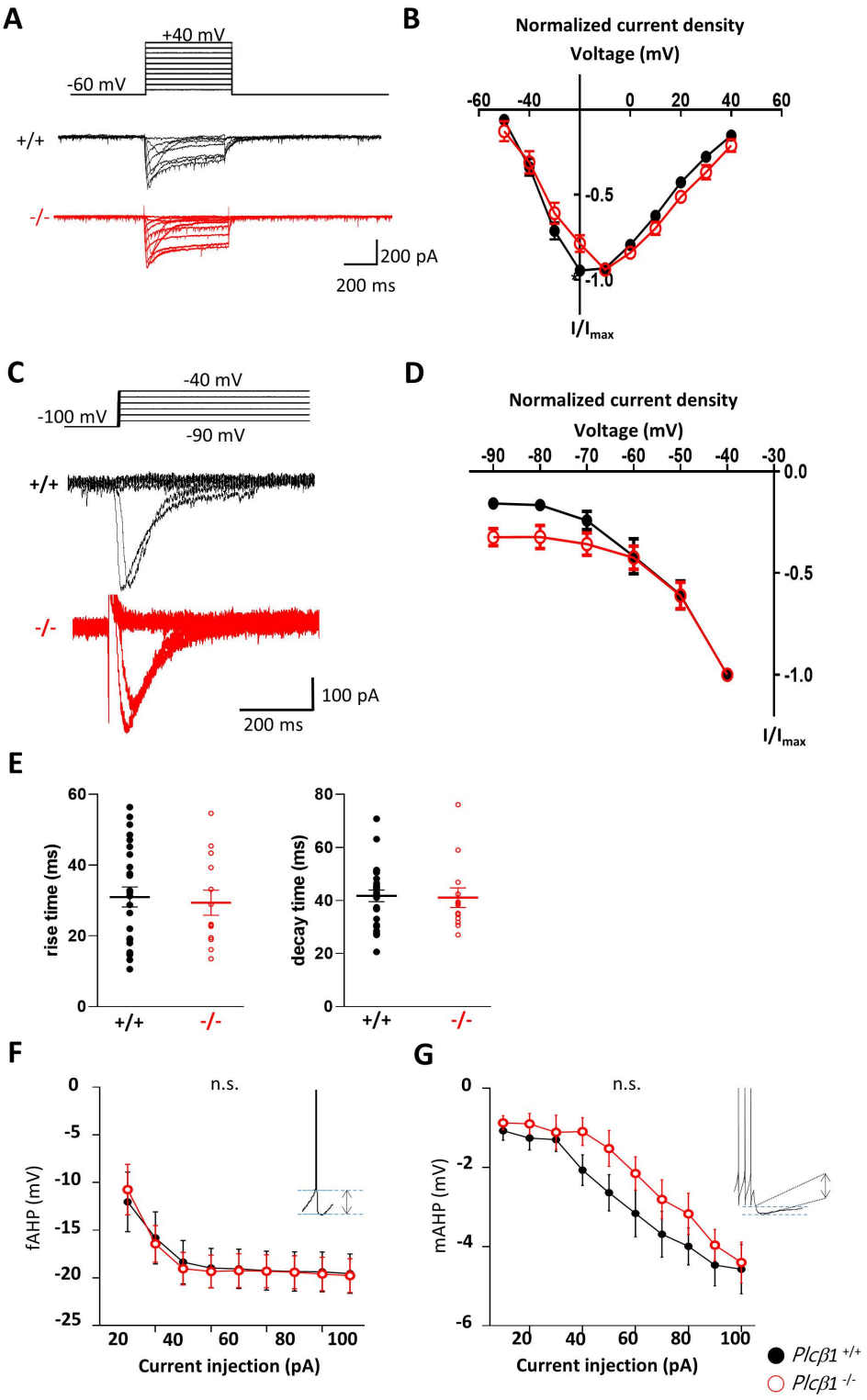

Fig. 6. Neither LVA nor HVA Ca^{2+} currents were changed in the vmTRNs of *Plcβ1*$^{-/-}$ mice. (A) Protocol for activating HVA Ca^{2+} channels (upper) and representative traces of HVA Ca^{2+} currents in *Plcβ1*$^{+/+}$ (middle) and *Plcβ1*$^{-/-}$ (lower) vmTRN neurons. (B) Summary graph of the normalized HVA current density (+/+, n=16, 9 mice; -/-, n=16, 6 mice). Two-tailed t test, $^{n.s.}$ p>0.92. (C) Protocol for activating LVA Ca^{2+} channels (upper) and representative traces of LVA Ca^{2+} currents in *Plcβ1*$^{+/+}$ (middle) and *Plcβ1*$^{-/-}$ (lower) vmTRN neurons. (D) Summary graph of the normalized LVA current density (+/+, n=31, 11 mice; -/-, n=17, 6 mice). Two-tailed t test, $^{n.s.}$ p>0.68. (E) LVA Ca^{2+} current rise time (left) and decay times (right) with in *Plcβ1*$^{+/+}$ and *Plcβ1*$^{-/-}$ mice. (F) Average fAHPs and (G) average mAHPs in *Plcβ1*$^{+/+}$ and *Plcβ1*$^{-/-}$ vmTRN neurons (+/+, n=30, 10 mice; -/-, n=15, 5 mice). Two-way ANOVA; multiple pairwise comparisons with a Bonferroni correction.

ized I~V curves between the two groups (Fig. 6B). These results indicate that HVA Ca^{2+} channels (L, P/Q-type) are not affected by the deletion of *Plcβ1* in the TRN.

Next, to assess LVA calcium currents, the TRN neurons were held at -60 mV as the resting membrane potential and deactivated by a hyperpolarizing prepulse step at -100 mV, followed by activation steps ranging from -90 to -40 mV. These steps activated LVA Ca^{2+} channels and induced the fast-inactivating current of T-type Ca^{2+} channels (Fig. 6C) [36]. The normalized I~V curves were unchanged by the peak density of a fast-inactivating current evoked at test potentials ranging from -90 to -40 mV in the TRN neurons of *Plcβ1*$^{-/-}$ mice compared to wild-type TRN neurons (Fig. 6D). We also observed LVA Ca^{2+} current decay times and rise time with wild and mutant mice. As a result, there was no significant difference between the two groups (Fig. 6E). These results imply that *Plcβ1* is not required for the activation of LVA Ca^{2+} currents. The conductance of calcium-activated potassium ion channels as well as low-threshold T-type calcium ion channels play an important role in TRN postinhibitory rebound bursts [37, 38] Thus, we focused on calcium-activated potassium conductance in the TRN neurons of *Plcβ1*$^{-/-}$ and wild-type mice. We determined whether the changes in SK and BK channels affected the action potential frequency by performing after hyperpolarization (AHP) analysis. The amplitude of fast AHP (fAHP) is caused by the activation of Ca^{2+}-activated large K^+ channels (BK channels), which play an important role in the repolarization of membrane potential after an action potential. These values did not significantly differ between *Plcβ1*$^{-/-}$ and wild-type neurons (Fig. 6F). Then, we examined the amplitude of the medium AHP (mAHP) caused by activation of Ca^{2+}-activated small K^+ channels (SK channels) and observed that mAHPs also did not differ in the mutant mice (Fig. 6G), indicating that Ca^{2+}dependent K^+ channels in the TRN neurons of *Plcβ1*$^{-/-}$ mice were normal. These results suggest that LVA and HVA Ca^{2+} currents are not involved in the reduced excitability of vmTRN neurons in *Plcβ1*$^{-/-}$ mice.

DISCUSSION

Plcβ1 deficiency is known to be associated with childhood epileptic encephalopathy, including absence seizures [23]. However, how and in which brain regions *Plcβ1* potentially plays a role in absence seizures were previously unknown. Our study revealed that the specific deletion of *Plcβ1* in the TRN is sufficient to generate absence seizures. In addition, the loss of *Plcβ1* function regulates the intrinsic excitability of TRN neurons in both tonic and burst firing modes, leading to cortex EEG signals and spontaneous absence seizures. This suggests that reductions in both tonic and burst firings in the TRN are concomitant with the induction of SWDs. We also found that the reduced tonic and burst firings were not mediated by the altered activity of low-threshold calcium channels or calcium-activated potassium ion channels. Taken together, our data suggest that *Plcβ1* deletion has unique mechanisms that modulate tonic and burst firing modes. This finding is the first clear demonstration of the role of *Plcβ1* in TRN neurons in absence seizure generation.

The patients with *Plcβ1* deficiency also had infantile spasms [24]. Hypsarrhythmia is the most common interictal EEG pattern associated with infantile spasms [39]. Hypsarrhythmia consists of chaotic, high-amplitude, mixed slow and sharp wave activity, sometimes combined with very fast oscillations (typically >70 Hz), which can be easily confused with SWDs in absence seizures [40, 41]. Therefore, in this study, we carefully examined EEG and EMG data to distinguish absence seizures from hypsarrhythmia. Regarding the EEG signals, our criteria for SWD included frequency as well as duration, amplitude, and peak-to-peak period. In addition, we carefully investigated the high frequency band after the event because hypsarrhythmia is often accompanied by transient fast gamma rhythms [42]. We found no transient fast gamma rhythms in *Plcβ1* knockout mice. Regarding the EMG signals, we found that *Plcβ1* knockout mice had reduced EMG signals during SWDs and did not show a rhomboid-shaped burst signal during or after absence seizures that differed from the EMG patterns found in infantile spasms [39]. Moreover, we did not observe an outward extension of the arms, a behavioral hallmark of infantile spasms [43], whereas we did find an arrest behavior indicative of absence seizures. In addition, EEG data obtained during sleep were excluded from the analysis because hypsarrhythmia is more likely to occur during NREM sleep [44]. Overall, we strongly believe that the criteria based on EEG and EMG signals to detect SWDs can distinguish between hypsarrhythmia and absence seizures and that the SWDs observed in this study represent only absence seizures.

Previous studies have demonstrated that patients with the *Plcβ1* gene may have a complex epileptic phenotype [22, 24]. A murine model of *Plcβ1*$^{-/-}$ presented with early generalized seizures and death, underscoring the role of *Plcβ1* in normal neuronal development and function [28]. More interestingly, in our study, whole-body *Plcβ1* KO mice on an F1 (B6jx129S4/SvJae) background, which show normal survival, exhibited complex-type seizures, including convulsive and absence seizures. However, when we specifically knocked down *Plcβ1* in the TRN, only SWDs, the hallmark of absence seizures, were observed. These data indicate that absence seizures associated with *Plcβ1* deficiency in humans may be closely related to PLCβ1 expression in the TRN. Convulsive

https://doi.org/10.5607/en22007

seizures in *Plcβ1*$^{-/-}$ mice may have been generated by other brain regions, such as the hippocampus, rather than the TRN. Indeed, it has been reported that the loss of *Plcβ1* function using transgene insertion in mice caused late-onset epileptic symptoms with aberrant mossy fiber sprouting in the hippocampus [45], where *Plcβ1* is highly expressed. Additionally, there is no direct projection from the TRN to the hippocampus. However, although there are no reports of a role of the TRN in convulsive seizures, the possibility of indirect regulation of the TRN in the hypersynchrony in the temporal lobe cannot be ruled out, and further investigation is needed. Taken together, our epilepsy model associated with the *Plcβ1* mutation establishes a path for further studies on the more detailed pathological causes of absence seizures in humans. Furthermore, here we report that the lack of *Plcβ1* in the TRN triggers the generation of absence seizures. For clinicians, such advances in genetic diagnosis can be highly beneficial.

Previously, we reported Plcβ4-deficient mice as a potential animal model for absence seizures [30, 46]. In terms of absence seizures, either Plcβ1 or Plcβ4 deficiency leads to absence seizures. Therefore, PLCβ1 and PLCβ4 are important for inducing absence seizures. However, there are clear differences between the two models in terms of brain targets and underlying mechanisms. In the thalamocortical circuit, PLCβ1 is mainly expressed in TRN neurons, whereas PLCβ4 is highly expressed in TC neurons [30]. Another important difference is that PLCβ4 modulates TC firing modes through simultaneous regulation of T- and L-type Ca^{2+} currents in TC neurons [34]. However, in the current study, we found no changes in T- and L-type Ca^{2+} currents in TRN neurons of *Plcβ1*$^{-/-}$ mice, indicating that PLCβ1 employs distinct cellular mechanisms to generate absence seizures. These data suggested that PLCβ1 and PLCβ4 modulate different downstream signaling pathways and targets to induce SWDs. Importantly, it is known that PLCβ1 and PLCβ4 utilize distinct signaling pathways by binding to specific types of receptors, such as the muscarinic receptor and type I metabotropic glutamate receptor 1 (mGluR1), respectively. For example, *Plcβ1*$^{-/-}$ mice exhibit major deficiencies in muscarinic-mediated PIP2 turnover without alterations in mGluR1-PIP2 turnover and show major developmental impairment and seizures through a loss of cortical developmental plasticity. In contrast, Plcβ4$^{-/-}$ mice have major deficits in mGluR1-mediated PIP2 turnover and induce several forms of neuroplasticity, such as developmental pruning of cerebellar ascending fibers, cerebellar LTD (long-term depression) induction), and forms of neuropathic pain [47]. Taken together, PLCβ1 in the TRN may modulate the neuronal excitability of TRN neurons through a unique cellular mechanism to induce absence seizures.

We observed reduced quantities of tonic firing in the TRN neurons of *Plcβ1*$^{-/-}$ mice. More importantly, in the same cells, we also found reduced burst firing. TRN bursts have long been implicated in the synchronization of and maintenance of thalamocortical oscillations, leading to spike-and-wave discharges (SWDs) [15, 16]. This view has been challenged by our previous study suggesting that enhanced TRN tonic firing in the absence of bursts in mice with *Cav3.3* KO or specific KD in the TRN is sufficient to generate SWDs, indicating the essential role of TRN tonic firing in the absence of TRN bursts for the absence seizure generation [13]. Another recent study by Makinson et al. [14] showed that reduced tonic firing without any alterations in burst firing in the TRNs of *Scn8a*$^{-/-}$ mice was associated with the absence of seizure generation confirming the role of tonic firing in TRN for absence seizure generation. Although discrepancies exist regarding the tonic firing behaviors of the TRN in each genetic mouse model (*Cav3.3*$^{-/-}$ and *Scn8a*$^{-/-}$) during absence seizure generation, we speculate that changes in the intrinsic excitability of the TRN are the most essential components for the modulation of TC circuit synchrony and the generation of absence seizures. However, the mechanisms by which the different tonic firing behaviors of TRN neurons from different genetic models (increased in *Cav3.3*$^{-/-}$ and decreased in *Scn8a*$^{-/-}$) lead to absence seizures remains unknown, and further studies are necessary to address this question.

Voltage-gated Ca^{2+} channels (VGCCs) and calcium-activated potassium channels play critical roles in the excitability of TRN neurons [13, 48]. Furthermore, LVA T-type calcium channels in particular are considered a key mechanism underlying the generation of burst firing [49]. In this study, we unexpectedly found that the properties of VGCCs and calcium-activated potassium channels were not altered in *Plcβ1*$^{-/-}$ TRN neurons, indicating that the reductions in tonic and burst firing in *Plcβ1*$^{-/-}$ KO mice were not due to changes in the activities of these calcium channels and potassium channels. Thus, we speculate that the TRN may promote absence seizures by blocking the voltage-gated sodium channels (VGSCs) associated with *Plcβ1*. A recent study reported that the loss of the sodium channel *Scn8a* (*NaV1.6*) from TRN cells preferentially impaired the excitation of action potentials (APs) and led to absence seizures [14]. Therefore, it is important to determine whether SCN8A plays any role in the reduced tonic firing in *Plcβ1*$^{-/-}$ mice.

Overall, while *Plcβ1* deficiency is known to be associated with childhood absence seizures, our study is the first to show that *Plcβ1* in the TRN plays an essential role in generating absence seizures in mice. Our results also revealed that the deletion of *Plcβ1* regulates the intrinsic excitability of TRN neurons. Therefore, in the future, understanding TRN-specific excitability via the control of tonic firing may be necessary to identify the mechanisms by which seizures are generated. Moreover, studying downstream

signaling molecules associated with *Plcβ1* may allow the identification of new targets for the treatment of absence seizures. These results highlight the previously unrealized importance of *Plcβ1* in the TRN for the generation of absence seizures.

ACKNOWLEDGEMENTS

This research was supported by the Institute for Basic Science (IBS), Center for Cognition and Sociality (IBS-R001-D2).

REFERENCES

1. Lerman P (1986) Seizures induced or aggravated by anticonvulsants. Epilepsia 27:706-710.
2. Beenhakker MP, Huguenard JR (2009) Neurons that fire together also conspire together: is normal sleep circuitry hijacked to generate epilepsy? Neuron 62:612-632.
3. Crunelli V, Leresche N (2002) Childhood absence epilepsy: genes, channels, neurons and networks. Nat Rev Neurosci 3:371-382.
4. Tenney JR, Glauser TA (2013) The current state of absence epilepsy: can we have your attention? Epilepsy Curr 13:135-140.
5. Lee HJ, Kim EH, Yum MS, Ko TS, Kim HW (2018) Attention profiles in childhood absence epilepsy compared with attention-deficit/hyperactivity disorder. Brain Dev 40:94-99.
6. Killory BD, Bai X, Negishi M, Vega C, Spann MN, Vestal M, Guo J, Berman R, Danielson N, Trejo J, Shisler D, Novotny EJ Jr, Constable RT, Blumenfeld H (2011) Impaired attention and network connectivity in childhood absence epilepsy. Neuroimage 56:2209-2217.
7. Bouma PA, Westendorp RG, van Dijk JG, Peters AC, Brouwer OF (1996) The outcome of absence epilepsy: a meta-analysis. Neurology 47:802-808.
8. Loiseau P, Pestre M, Dartigues JF, Commenges D, Barberger-Gateau C, Cohadon S (1983) Long-term prognosis in two forms of childhood epilepsy: typical absence seizures and epilepsy with rolandic (centrotemporal) EEG foci. Ann Neurol 13:642-648.
9. Huguenard JR, McCormick DA (2007) Thalamic synchrony and dynamic regulation of global forebrain oscillations. Trends Neurosci 30:350-356.
10. Clemente-Perez A, Makinson SR, Higashikubo B, Brovarney S, Cho FS, Urry A, Holden SS, Wimer M, Dávid C, Fenno LE, Acsády L, Deisseroth K, Paz JT (2017) Distinct thalamic reticular cell types differentially modulate normal and pathological cortical rhythms. Cell Rep 19:2130-2142.
11. Li Y, Lopez-Huerta VG, Adiconis X, Levandowski K, Choi S, Simmons SK, Arias-Garcia MA, Guo B, Yao AY, Blosser TR, Wimmer RD, Aida T, Atamian A, Naik T, Sun X, Bi D, Malhotra D, Hession CC, Shema R, Gomes M, Li T, Hwang E, Krol A, Kowalczyk M, Peça J, Pan G, Halassa MM, Levin JZ, Fu Z, Feng G (2020) Distinct subnetworks of the thalamic reticular nucleus. Nature 583:819-824.
12. Jones EG (2012) The thalamus. Springer Science & Business Media, New York, NY.
13. Lee SE, Lee J, Latchoumane C, Lee B, Oh SJ, Saud ZA, Park C, Sun N, Cheong E, Chen CC, Choi EJ, Lee CJ, Shin HS (2014) Rebound burst firing in the reticular thalamus is not essential for pharmacological absence seizures in mice. Proc Natl Acad Sci U S A 111:11828-11833.
14. Makinson CD, Tanaka BS, Sorokin JM, Wong JC, Christian CA, Goldin AL, Escayg A, Huguenard JR (2017) Regulation of thalamic and cortical network synchrony by Scn8a. Neuron 93:1165-1179.e6.
15. Cheong E, Shin HS (2013) T-type Ca2+ channels in normal and abnormal brain functions. Physiol Rev 93:961-992.
16. Huguenard JR (1996) Low-threshold calcium currents in central nervous system neurons. Annu Rev Physiol 58:329-348.
17. De Camilli P, Emr SD, McPherson PS, Novick P (1996) Phosphoinositides as regulators in membrane traffic. Science 271:1533-1539.
18. Hannan AJ, Blakemore C, Katsnelson A, Vitalis T, Huber KM, Bear M, Roder J, Kim D, Shin HS, Kind PC (2001) PLC-beta1, activated via mGluRs, mediates activity-dependent differentiation in cerebral cortex. Nat Neurosci 4:282-288.
19. Suh PG, Park JI, Manzoli L, Cocco L, Peak JC, Katan M, Fukami K, Kataoka T, Yun S, Ryu SH (2008) Multiple roles of phosphoinositide-specific phospholipase C isozymes. BMB Rep 41:415-434.
20. Caricasole A, Sala C, Roncarati R, Formenti E, Terstappen GC (2000) Cloning and characterization of the human phosphoinositide-specific phospholipase C-beta 1 (PLC beta 1). Biochim Biophys Acta 1517:63-72.
21. Montaña M, García del Caño G, López de Jesús M, González-Burguera I, Echeazarra L, Barrondo S, Sallés J (2012) Cellular neurochemical characterization and subcellular localization of phospholipase C β1 in rat brain. Neuroscience 222:239-268.
22. Poduri A, Chopra SS, Neilan EG, Elhosary PC, Kurian MA, Meyer E, Barry BJ, Khwaja OS, Salih MA, Stödberg T, Scheffer IE, Maher ER, Sahin M, Wu BL, Berry GT, Walsh CA, Picker J, Kothare SV (2012) Homozygous PLCB1 deletion associated

with malignant migrating partial seizures in infancy. Epilepsia 53:e146-e150.
23. Kurian MA, Meyer E, Vassallo G, Morgan NV, Prakash N, Pasha S, Hai NA, Shuib S, Rahman F, Wassmer E, Cross JH, O'Callaghan FJ, Osborne JP, Scheffer IE, Gissen P, Maher ER (2010) Phospholipase C beta 1 deficiency is associated with early-onset epileptic encephalopathy. Brain 133:2964-2970.
24. Ngoh A, McTague A, Wentzensen IM, Meyer E, Applegate C, Kossoff EH, Batista DA, Wang T, Kurian MA (2014) Severe infantile epileptic encephalopathy due to mutations in PLCB1: expansion of the genotypic and phenotypic disease spectrum. Dev Med Child Neurol 56:1124-1128.
25. Kim D, Jun KS, Lee SB, Kang NG, Min DS, Kim YH, Ryu SH, Suh PG, Shin HS (1997) Phospholipase C isozymes selectively couple to specific neurotransmitter receptors. Nature 389:290-293.
26. Lovett-Barron M, Turi GF, Kaifosh P, Lee PH, Bolze F, Sun XH, Nicoud JF, Zemelman BV, Sternson SM, Losonczy A (2012) Regulation of neuronal input transformations by tunable dendritic inhibition. Nat Neurosci 15:423-430, S1-S3.
27. Royer S, Zemelman BV, Losonczy A, Kim J, Chance F, Magee JC, Buzsáki G (2012) Control of timing, rate and bursts of hippocampal place cells by dendritic and somatic inhibition. Nat Neurosci 15:769-775.
28. Kim SW, Seo M, Kim DS, Kang M, Kim YS, Koh HY, Shin HS (2015) Knockdown of phospholipase C-β1 in the medial prefrontal cortex of male mice impairs working memory among multiple schizophrenia endophenotypes. J Psychiatry Neurosci 40:78-88.
29. Richards DA, Manning JP, Barnes D, Rombola L, Bowery NG, Caccia S, Leresche N, Crunelli V (2003) Targeting thalamic nuclei is not sufficient for the full anti-absence action of ethosuximide in a rat model of absence epilepsy. Epilepsy Res 54:97-107.
30. Cheong E, Zheng Y, Lee K, Lee J, Kim S, Sanati M, Lee S, Kim YS, Shin HS (2009) Deletion of phospholipase C beta4 in thalamocortical relay nucleus leads to absence seizures. Proc Natl Acad Sci U S A 106:21912-21917.
31. Arai R, Jacobowitz DM, Deura S (1994) Distribution of calretinin, calbindin-D28k, and parvalbumin in the rat thalamus. Brain Res Bull 33:595-614.
32. Hou G, Smith AG, Zhang ZW (2016) Lack of intrinsic GABAergic connections in the thalamic reticular nucleus of the mouse. J Neurosci 36:7246-7252.
33. Lee SH, Govindaiah G, Cox CL (2007) Heterogeneity of firing properties among rat thalamic reticular nucleus neurons. J Physiol 582(Pt 1):195-208.
34. Cheong E, Lee S, Choi BJ, Sun M, Lee CJ, Shin HS (2008) Tuning thalamic firing modes via simultaneous modulation of T- and L-type Ca2+ channels controls pain sensory gating in the thalamus. J Neurosci 28:13331-13340.
35. Zaman T, Lee K, Park C, Paydar A, Choi JH, Cheong E, Lee CJ, Shin HS (2011) Cav2.3 channels are critical for oscillatory burst discharges in the reticular thalamus and absence epilepsy. Neuron 70:95-108.
36. Fox AP, Nowycky MC, Tsien RW (1987) Kinetic and pharmacological properties distinguishing three types of calcium currents in chick sensory neurones. J Physiol 394:149-172.
37. Sanchez-Vives MV, Bal T, McCormick DA (1997) Inhibitory interactions between perigeniculate GABAergic neurons. J Neurosci 17:8894-8908.
38. Deleuze C, Huguenard JR (2006) Distinct electrical and chemical connectivity maps in the thalamic reticular nucleus: potential roles in synchronization and sensation. J Neurosci 26:8633-8645.
39. Scantlebury MH, Galanopoulou AS, Chudomelova L, Raffo E, Betancourth D, Moshé SL (2010) A model of symptomatic infantile spasms syndrome. Neurobiol Dis 37:604-612.
40. Kellaway P, Hrachovy RA, Frost JD Jr, Zion T (1979) Precise characterization and quantification of infantile spasms. Ann Neurol 6:214-218.
41. Traub RD, Moeller F, Rosch R, Baldeweg T, Whittington MA, Hall SP (2020) Seizure initiation in infantile spasms vs. focal seizures: proposed common cellular mechanisms. Rev Neurosci 31:181-200.
42. Kobayashi K, Miya K, Akiyama T, Endoh F, Oka M, Yoshinaga H, Ohtsuka Y (2013) Cortical contribution to scalp EEG gamma rhythms associated with epileptic spasms. Brain Dev 35:762-770.
43. Panayiotopoulos (2005) The epilepsies: seizures, syndromes and management. Bladon Medical Publishing, Oxfordshire.
44. Watanabe K, Negoro T, Aso K, Matsumoto A (1993) Reappraisal of interictal electroencephalograms in infantile spasms. Epilepsia 34:679-685.
45. Böhm D, Schwegler H, Kotthaus L, Nayernia K, Rickmann M, Köhler M, Rosenbusch J, Engel W, Flügge G, Burfeind P (2002) Disruption of PLC-beta 1-mediated signal transduction in mutant mice causes age-dependent hippocampal mossy fiber sprouting and neurodegeneration. Mol Cell Neurosci 21:584-601.
46. Lee S, Hwang E, Lee M, Choi JH (2019) Distinct topographical patterns of spike-wave discharge in transgenic and pharmacologically induced absence seizure models. Exp Neurobiol 28:474-484.

47. Sossin WS, Farah CA (2009) Synaptic plasticity: diacylglycerol signalling role. In: Encyclopedia of neuroscience (Squire LR, ed), pp 747-755. Academic Press, Oxford.
48. Cueni L, Canepari M, Luján R, Emmenegger Y, Watanabe M, Bond CT, Franken P, Adelman JP, Lüthi A (2008) T-type Ca2+ channels, SK2 channels and SERCAs gate sleep-related oscillations in thalamic dendrites. Nat Neurosci 11:683-692.
49. Bal T, von Krosigk M, McCormick DA (1995) Synaptic and membrane mechanisms underlying synchronized oscillations in the ferret lateral geniculate nucleus in vitro. J Physiol 483(Pt 3):641-663.

https://doi.org/10.5607/en22007